Journal of Materials Chemistry A

PAPER

View Article Online
View Journal

Cite this: DOI: 10.1039/c9ta04643g

High yield electrochemical exfoliation synthesis of tin selenide quantum dots for high-performance lithium-ion batteries†

Jing Li,[ab] Wei Liu,[b] Cheng Chen,[b] Xiaoxu Zhao,[c] Zhizhan Qiu,[bd] Haomin Xu,[b] Feng Sheng,[e] Qifeng Hu,[e] Yi Zheng,[e] Ming Lin,[f] Stephen J. Pennycook,[c] Chenliang Su *[a] and Jiong Lu*[bg]

Received 4th May 2019
Accepted 5th July 2019

DOI: 10.1039/c9ta04643g

rsc.li/materials-a

Tin selenide (SnSe) nanostructures hold great promise as an anode material in lithium-ion batteries (LIBs) due to their high storage capacity, rapid lithiation kinetics and long-term cycling stability. However, a scalable synthesis of SnSe nanostructures with a well-defined size remains a challenge in chemistry. Here, we report cathodic exfoliation of a bulk SnSe crystal for a high-yield (>90%) synthesis of sub-5 nm scale SnSe quantum dots (QDs). As-exfoliated SnSe QDs demonstrate a superior performance as the anode material for LIBs. Our results reveal that SnSe QDs not only accommodate the volume expansion/contraction during the reversible charging/discharging in LIBs but also increase the effective contact interface area between the nanostructured anode materials and electrolyte, leading to a high charging/discharging rate and superior cycling performance. Additionally, SnSe QD based LIBs exhibit a reversible capacity retention of 550 mA h g^{-1} and high coulombic efficiency approaching 100% after 1500 charging/discharging cycles at a current density of 0.5 A g^{-1}.

Dr Jiong Lu is currently an assistant professor at Department of Chemistry, Centre for Advanced 2D Materials, at National University of Singapore (NUS). He received his Bachelor's degree from Fudan University (China) in 2007 and Ph.D. degree from NUS in 2011. After that, he worked as a postdoc fellow in Graphene Research Centre, NUS and then joined Mike Crommie's group at Department of Physics, UC, Berkeley for his postdoctoral research. His current research interests include atomic-scale imaging and characterization of 2D materials and their gate-tunable devices, and single-atom catalysis for energy related applications. He has published more than 40 peer-reviewed papers with a total of over 3700 citations.

Introduction

Tin selenide (SnSe), a IV–VI group semiconductor consisting of earth abundant and environmentally benign elements, has recently gained a renewed interest owing to its outstanding electronic and thermoelectric properties.[1–4] In addition, SnSe is also predicted to be a promising anode material in LIBs with high theoretical storage capacity[5] and rapid lithiation kinetics due to its excellent electrical conductivity and unique puckered structures.[6] Downsizing the bulk SnSe into nanosized structures not only increases the surface-to-volume ratio but also favours the decomposition of Li_2Se, leading to an enhanced capacity and cycling performance.[7–10] Unfortunately, a facile approach for the scalable synthesis of nanostructured SnSe materials with a controlled size for high-performance LIBs is still lacking.

To date, colloidal synthesis has been a major route for the fabrication of SnSe nanostructures. Apart from the use of toxic and air-sensitive Se precursors,[11–14] it also remains a great

[a]SZU-NUS Collaborative Center, International Collaborative Laboratory of 2D Materials for Optoelectronic Science & Technology of Ministry of Education, Engineering Technology Research Center for 2D Materials Information Functional Devices and Systems of Guangdong Province, Institute of Microscale Optoelectronics, Shenzhen University, Shen Zhen, 518060, China. E-mail: chmsuc@szu.edu.cn

[b]Department of Chemistry, National University of Singapore, 3 Science Drive 3, Singapore 117543. E-mail: chmluj@nus.edu.sg

[c]Department of Materials Science and Engineering, National University of Singapore, 9 Engineering Drive 1, 117575, Singapore

[d]NUS Graduate School for Integrative Sciences and Engineering, National University of Singapore, 28 Medical Drive, Singapore 117456, Singapore

[e]Department of Physics, Zhejiang University, Hangzhou 310027, China

[f]Institute of Materials Research and Engineering, Agency for Science, Technology and Research (A*STAR), 2 Fusionopolis Way, Innovis, #08-03, Singapore 138634

[g]Centre for Advanced 2D Materials, Graphene Research Centre, National University of Singapore, Singapore 117546

† Electronic supplementary information (ESI) available. See DOI: 10.1039/c9ta04643g

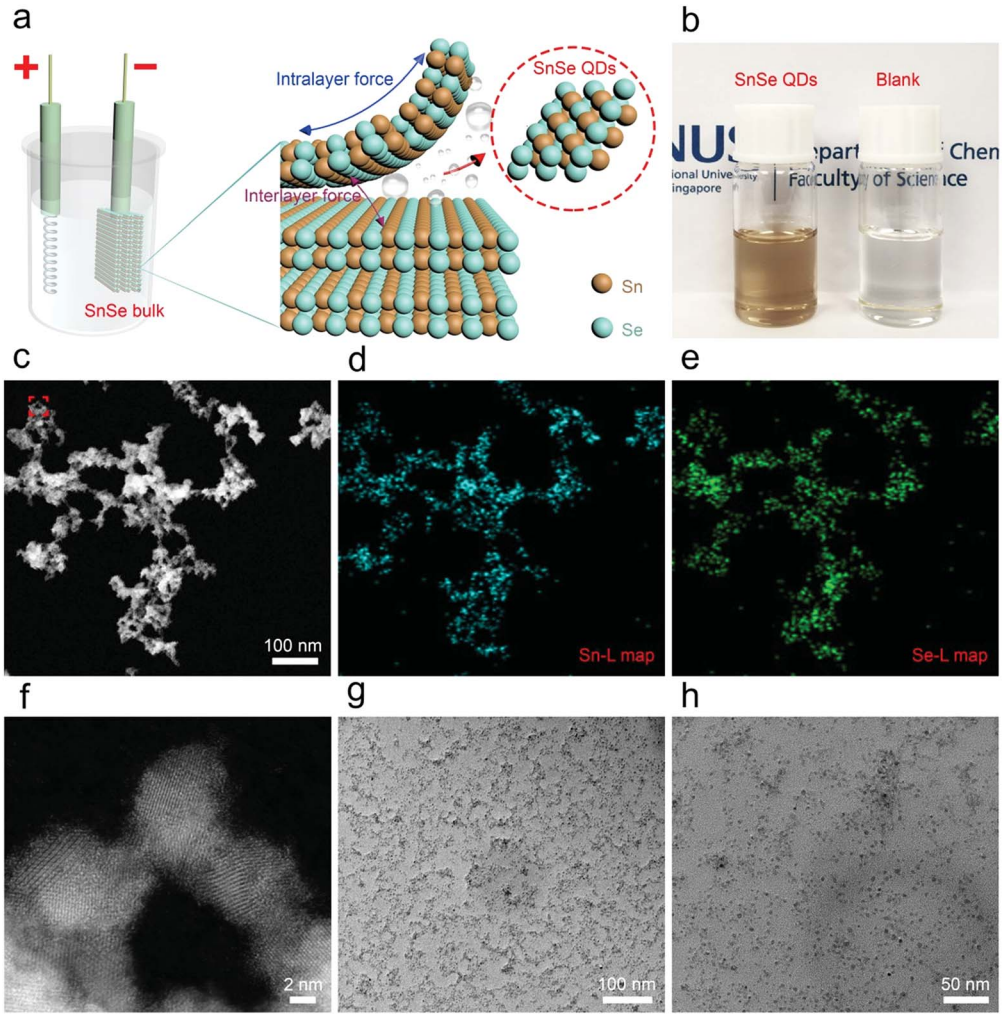

Fig. 1 Schematic illustration of the electrochemical exfoliation method and structural characterization of SnSe QDs. (a) Schematic illustration of the synthesis of SnSe QDs by cathodic exfoliation. (b) Photograph of SnSe QDs dispersion and blank electrolyte. (c) STEM-ADF images and the corresponding (d and e) STEM-EELS mapping of exfoliated SnSe QDs. Sn and Se are shown in cyan and green respectively. (f) Atomic-resolution STEM images of SnSe regions marked in panel (c). (g) Large-area and (h) close-up TEM images of isolated SnSe QDs after sonication.

challenge to control the composition and structural phase of SnSe nanocrystals arising from the stringent reaction conditions and the oxidation tendency of Sn(II) in air.[15,16] In contrast to bottom-up colloidal synthesis,[5,12,17–19] top-down exfoliation of SnSe bulk materials into SnSe nanostructures appears as a more promising alternative due to its remarkable efficiency, high scalability and low cost.[20–22] Here, we report a facile cathodic exfoliation approach for the effective downsizing of bulk SnSe into SnSe quantum dots (QDs) with controlled sizes by using tetra-butylammonium (TBA) cations as intercalants. It is observed that intercalated TBA cations undergo electrochemical decomposition at cathodic potential, leading to quasi-isotropic exfoliation of bulk SnSe crystals along in-plane and out-of-plane directions. This enables a high yield production of SnSe QDs with an average lateral-size/vertical-thickness of ~3.8/1.7 nm. We also demonstrated that SnSe QDs can be used as an excellent anode material with superior performance and stability in LIBs.

Results and discussion

Orthorhombic SnSe shares the same puckered structure as black phosphorus (BP) but with a much stronger interlayer coupling strength. Inspired by the electrochemical exfoliation of black phosphorus,[23] bulk SnSe was cathodically charged in a two electrode electrochemical cell with a Pt wire as a counter electrode in an organic electrolyte consisting of 0.05 M TBA cations in propylene carbonate (PC) (Fig. 1a). Although bulk SnSe exhibits negligible volume expansion after applying a voltage of −5 V for 30 min, we observed that the tiny flakes were delaminated from the cathode surface and the resulting electrolyte evolved from colourless to brown. Transmission electron microscopy (TEM) images reveal that the exfoliated materials consist of a few-layer SnSe nanostructure with a size ranging from 5 to 30 nm (Fig. S2†).

To further downsize the SnSe nanostructure, a more rigorous intercalation condition (−7.5 V) was applied to exfoliate bulk

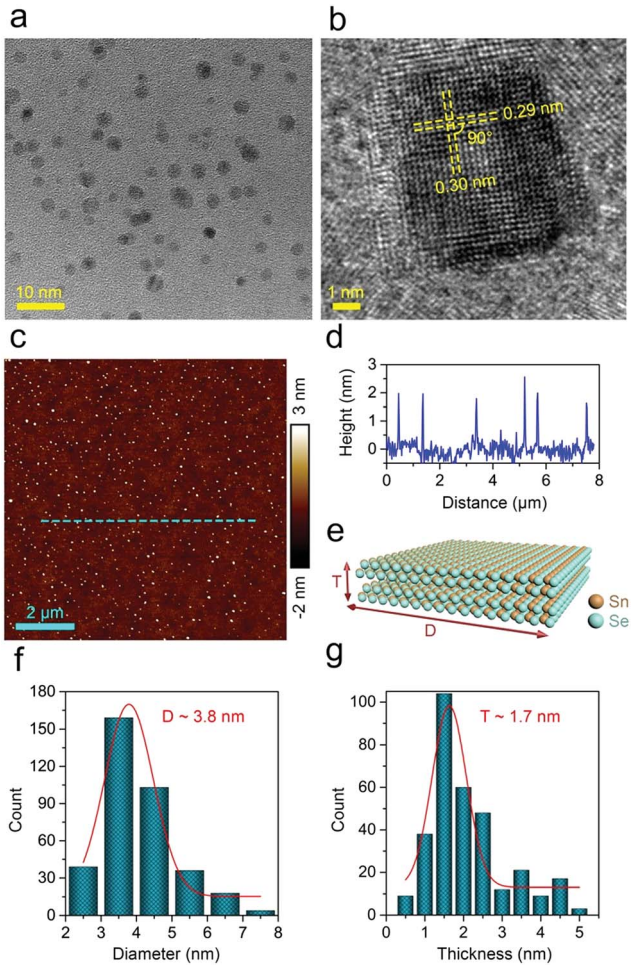

Fig. 2 Structural and morphology characterization of SnSe QDs. (a) TEM, (b) HRTEM and (c) AFM images of SnSe QDs. (d) Height profile along the dashed line marked in panel (c). Statistical analysis of the size and thickness of SnSe QDs (structural model is shown in panel (e)) with (f) lateral diameter and (g) vertical thickness as measured by TEM and AFM, respectively.

SnSe in an electrolyte with a relatively high concentration of 0.2 M TBA. Under this exfoliation condition, small fragments peeled off from the bulk SnSe in a more rapid manner (Fig. S4†). The atomic-resolution scanning transmission electron microscopy-annular dark field (STEM-ADF) image in Fig. 1c reveals that the exfoliated SnSe materials are composed of nanodots with a lateral size less than 10 nm, which can be regarded as quantum dots (QDs) (Fig. S5†). In addition, electron energy loss spectroscopy (EELS) mapping reveals a uniform distribution of Sn and Se in the exfoliated SnSe QDs (Fig. 1c–e). With a bath sonication at 100 W for 10 min, the weakly entangled nanodots can be easily separated into isolated QDs with a smaller lateral dimension (~4 nm) as shown in Fig. 1g and h.

High resolution TEM was employed to evaluate the size and morphology of well-separated SnSe QDs. The TEM image in Fig. 2a shows that the size of as-obtained SnSe QDs is of several nanometers. The HR-TEM image (Fig. 2b) captured the orthorhombic lattice of SnSe with a spacing of ~0.3 nm and an intersection angle of ~90°, consistent with the (011) plane of SnSe.[18,24] We also conducted atomic force microscopy (AFM) to further characterize the dimension and morphology of exfoliated SnSe QDs (Fig. 2c).

The representative AFM height profile (Fig. 2d) demonstrates that the thickness of SnSe QDs is ~2 nm. Based on the statistical analysis of ~300 SnSe QDs imaged by TEM and AFM, the average lateral diameter and vertical thickness are determined to be 3.8 ± 1.25 nm and 1.7 ± 0.6 nm (3–4 layers of SnSe) respectively.[25]

We note that the cathodic exfoliation of bulk BP produces large-sized thin sheets rather than QD structures under similar exfoliation conditions in the previous report.[23] Such a dramatic difference in the exfoliation of SnSe and BP could be associated with the different interlayer and intralayer bonding strength in these two different materials. To better understand this, we conducted low-temperature scanning tunnelling microscopy (STM) imaging of bulk SnSe. It is found that multiple vacancies can be created due to the breakage of Sn–Se bonding by sweeping sample bias from 1.4 V to −1.2 V during STM spectroscopic measurements (Fig. 3a and b). In addition, we also observed the detachment of SnSe at the step edges during STM spectroscopic measurement. As shown in Fig. 3c and d, a SnSe domain with a size of ~5 nm is removed from the step edge. In contrast, such a bond breakage is absent for bulk BP under similar conditions. These observations indicate a weaker in-

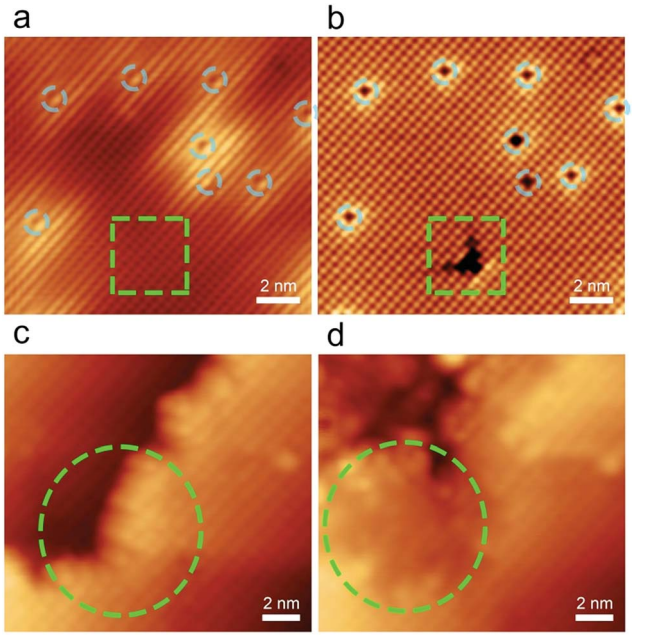

Fig. 3 The breakage of in-plane Sn–Se bonding during STM spectroscopic measurement. STM images of the intact SnSe area (a) before and (b) after the voltage sweeping from 1.4 to −1.2 V. Blue dashed circles denote the intrinsic defects in bulk SnSe, and green dashed boxes represent as-formed defects during STM spectroscopic measurements. STM images of the step edge of bulk SnSe (c) before and (d) after the voltage sweeping from 1.4 to −1.2 V, and the detached SnSe area is marked by a green dashed circle. Tunnelling parameters: $V_s = 1.5$ V, $I = 0.8$ nA (a); $V_s = -1.85$ V, $I = 0.6$ nA (b); $V_s = -2.05$ V, $I = 0.6$ nA (c); $V_s = -2.05$ V, $I = 0.6$ nA (d).

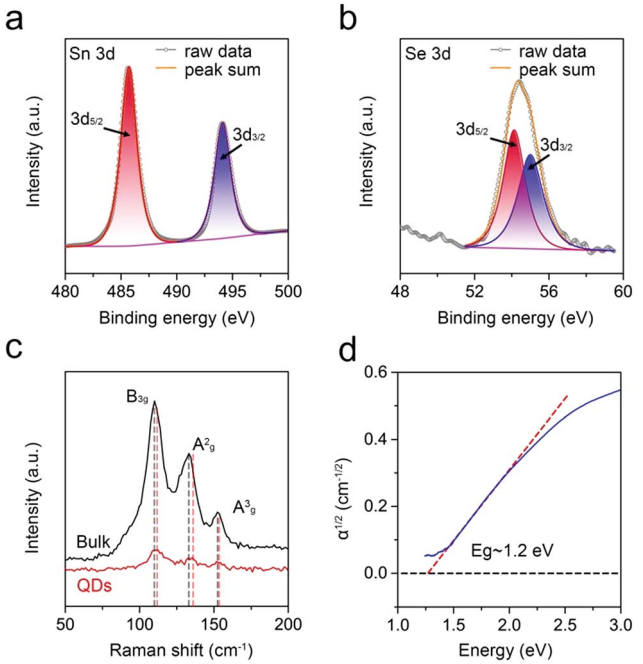

Fig. 4 Chemical composition and optical properties of SnSe QDs. High-resolution XPS spectra of (a) Sn 3d and (b) Se 3d of SnSe QDs. (c) Raman spectra of SnSe QDs and the bulk crystal. (d) Tauc plot of $(\alpha h\nu)^{1/2}$ as a function of photon energy of SnSe QDs dispersed in PC solvent. α is the measured adsorption coefficient from the UV-vis absorption spectrum.

plane bonding strength of SnSe compared to that of BP.[26,27] Moreover, density functional theory (DFT) calculation also predicts that the interlayer bonding energy of SnSe is about 1.5 times larger than that of BP.[28,29] The strong interlayer bonding in combination with a relatively weaker intralayer bonding causes SnSe to differ from conventional 2D layered materials, resulting in quasi-isotropic exfoliation for the synthesis of SnSe QDs.

To probe the structure and chemical composition of as-exfoliated QDs, we performed X-ray photoelectron spectroscopy (XPS) and Raman spectroscopy measurements. As revealed in Fig. 4a and b, the high resolution Sn 3d spectrum shows two peaks at 485.7 eV ($3d_{5/2}$) and 494.1 eV ($3d_{3/2}$), attributed to the Sn(II).[16] In addition, Se $3d_{5/2}$ and $3d_{3/2}$ related features are found to peak at 54.1 eV and 55.0 eV, respectively.[30] The absence of a high oxidation state of Sn (*e.g.*, Sn(IV)) further supports that cathodic exfoliation can prevent material oxidation during the electrochemical delamination process. Three characteristic Raman peaks at 107.8, 130.7 and 151.1 cm^{-1} of as-synthesized QDs can be ascribed to the B_{3g}, A_g^2 and A_g^3 phonon mode of SnSe, respectively.[31,32] It is noted that these Raman peaks acquired over SnSe QDs show a red shift compared with that of bulk SnSe (Fig. 4c), which arises from the reduced dimensional effect as reported in other QD materials such as BP[33] and transition metal dichalcogenides.[34] The optical properties of SnSe QDs were also investigated by UV-vis spectroscopy (Fig. S6†). As shown in Fig. 4d, a standard fitting of Tauc's plot

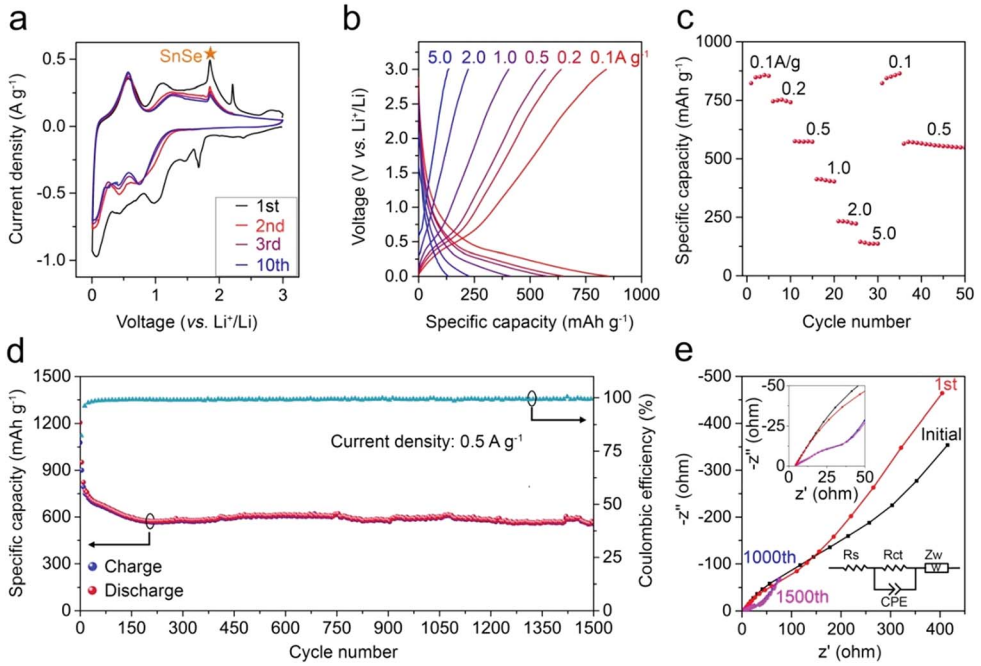

Fig. 5 Electrochemical performance of SnSe QDs as the anode material for lithium storage in half-cells. (a) CV curves for the initial cycles of SnSe QDs at a scanning rate of 0.1 mV s^{-1}. (b) Galvanostatic charging–discharging profiles and (c) rate capability of SnSe QDs at different current densities. (d) Cycle performance and (e) EIS spectra of SnSe QDs after fully charging/discharging cycles at a current density of 0.5 A g^{-1} for a long-term cycling. Upper inset is the zoom-in EIS spectra at high frequency. Lower inset is the equivalent circuit used to fit the experimental data. R_s is the intersection point of the semicircle with the real axis at high frequency, corresponding to a sum of all ohmic resistances from the electrode and the electrolyte. R_{ct} is the diameter of the semicircle at middle frequency, ascribed to the charge-transfer resistance at the interface. CPE is the constant phase element for the capacitance coupled with R_{ct}. Z_w represents the diffusion impedance (Warburg impedance).

of $(\alpha h\nu)^{1/2}$ *versus* photon energy yields an indirect bandgap of ~1.2 eV for SnSe QDs dispersed in PC solvent, consistent with the bandgap reported for SnSe QDs synthesized by colloidal synthesis.[14]

The electrochemical performance of as-exfoliated SnSe QDs was evaluated by performing cyclic voltammetry (CV) and galvanostatic charge–discharge in combination with the metallic Li counter electrode in a coin-type half-cell. The CV curves for the first few cycles at a scanning rate of 0.1 mV s^{-1} are shown in Fig. 5a. The observation of cathodic peaks at 1.46 V and 1.68 V and the anodic peak at 2.21 V in the first sweep can be ascribed to the formation of a solid electrolyte interface (SEI) layer on the electrode.[35] In the subsequent CV cycles, the cathodic peak around 0.80 V is attributed to the reaction of SnSe with Li to form Li_2Se and Sn, while the peak around 0.44 V is ascribed to the alloying between Sn and Li. The reduction peak at 0.56 V arises from the dealloying of Li_xSn. The peak around 1.85 V (Fig. S7†) is associated with the reactions between Li_2Se and Sn to form SnSe.[35] Moreover, the re-emergence of these features in the multiple cycling test confirms that SnSe QDs undergo reversible lithium intercalation and de-intercalation for LIBs.

We carried out the galvanostatic test to further investigate the charging–discharging rate performance of SnSe QDs at various current densities ranging from 0.1 to 5 A g^{-1} (Fig. 5b and c). SnSe QDs can deliver an initial capacity of 830 mA h g^{-1} at the current density of 0.1 A g^{-1}, and exhibit a high cycling stability at all the current densities, including a large current density of 5 A g^{-1}. In particular, a specific capacity of 830 mA h g^{-1} (approaching the theoretical capacity of 847 mA h g^{-1})[36] of the SnSe anode can be restored and remains stable when the battery is cycled back from 5 A g^{-1} to 0.1 A g^{-1}. This further indicates the SnSe QDs as the anode material remain stable even after a high rate cycling test.

The long-term cycling instability has been one of the major issues for IV–VI compound based anode materials.[37–39] Here, the SnSe QDs demonstrate a remarkable cycling stability with a discharged capacity retention of 550 mA h g^{-1} after 1500 charging/discharging cycles at 0.5 A g^{-1}. The extraordinary cycling stability of SnSe QDs can be attributed to the increased surface area and buffering capability of nano-sized structures that can accommodate the large volume expansion/contraction. Moreover, the reversible conversion of Li_2Se also contributes to the reversible formation of SnSe, leading to a further enhancement of battery capacity.

The electrochemical impedance spectra (EIS) of SnSe QDs under open circuit voltage (OCV) for LIBs were measured with a frequency range from 100 kHz to 1 Hz as shown in Fig. 5e. The formation of the SEI film will alter the contact resistance at high frequency, and the charge-transfer process in the middle-frequency, which will alter the semicircle in Nyquist plots. The linear increase in the low-frequency range reflects Warburg impedance associated with lithium ion diffusion into the SnSe QD anode.[40–42] In contrast to one depressed semicircle (fitted charge-transfer resistance $R_{ct} \sim 249\ \Omega$) at high frequencies before cycling, two semicircles corresponding to the resistance contributed by the SEI film (~17 Ω) and the charge-transfer process ($R_{ct} \sim 103\ \Omega$) appear after running multiple charging/discharging cycles. This indicates that an enhanced electrical conductivity facilitates the charge transfer process after the formation of a stable SEI film. In addition, an increased effective contact area between SnSe QDs and electrolyte can shorten the ion diffusion and transport pathways, which thus enables a high rate charging/discharging capability.

Conclusions

In summary, we have devised highly efficient electrochemical exfoliation of bulk SnSe crystals for a high yield synthesis (>90% yield) of sub-5 nm sized SnSe QDs as the anode material in lithium-ion batteries. Our results demonstrate that reducing the size of SnSe into the nanoscale not only facilitates the reversible Li insertion/extraction for high cycling stability but also improves the host storage capacity. Moreover, the lithium-ion battery shows a reversible capacity retention of 550 mA h g^{-1} after 1500 charging/discharging cycles at a current density of 0.5 A g^{-1}. Our findings offer a new route for the synthesis of low dimensional SnSe nanostructures for both fundamental study and practical applications.

Conflicts of interest

There are no conflicts to declare.

Acknowledgements

The authors acknowledge the support from the National Natural Science Foundation of China (21703143, 11574264), MOE grants (R-143-000-682-112, R-143-000-A06-112 and R-143-000-A75-114), Shenzhen Peacock Plan (Grant No. KQJSCX20170727100802505 and KQTD2016053112042971), the Educational Commission of Guangdong Province (2016KCXTD006), and the Guangdong Special Support Program.

References

1 L.-D. Zhao, S.-H. Lo, Y. Zhang, H. Sun, G. Tan, C. Uher, C. Wolverton, V. P. Dravid and M. G. Kanatzidis, *Nature*, 2014, **508**, 373–377.
2 L.-D. Zhao, G. Tan, S. Hao, J. He, Y. Pei, H. Chi, H. Wang, S. Gong, H. Xu, V. P. Dravid, C. Uher, G. J. Snyder, C. Wolverton and M. G. Kanatzidis, *Science*, 2016, **351**, 141–144.
3 L.-D. Zhao, V. P. Dravid and M. G. Kanatzidis, *Energy Environ. Sci.*, 2014, **7**, 251–268.
4 Z. Wang, C. Fan, Z. Shen, C. Hua, Q. Hu, F. Sheng, Y. Lu, H. Fang, Z. Qiu, J. Lu, Z. Liu, W. Liu, Y. Huang, Z.-A. Xu, D. W. Shen and Y. Zheng, *Nat. Commun.*, 2018, **9**, 47.
5 G. Han, S. R. Popuri, H. F. Greer, J.-W. G. Bos, W. Zhou, A. R. Knox, A. Montecucco, J. Siviter, E. A. Man, M. Macauley, D. J. Paul, W.-g. Li, M. C. Paul, M. Gao, T. Sweet, R. Freer, F. Azough, H. Baig, N. Sellami, T. K. Mallick and D. H. Gregory, *Angew. Chem., Int. Ed.*, 2016, **55**, 6433–6437.

6 J. Sun, H.-W. Lee, M. Pasta, H. Yuan, G. Zheng, Y. Sun, Y. Li and Y. Cui, *Nat. Nanotechnol.*, 2015, **10**, 980.
7 Y.-G. Guo, J.-S. Hu and L.-J. Wan, *Adv. Mater.*, 2008, **20**, 2878–2887.
8 W.-M. Zhang, J.-S. Hu, Y.-G. Guo, S.-F. Zheng, L.-S. Zhong, W.-G. Song and L.-J. Wan, *Adv. Mater.*, 2008, **20**, 1160–1165.
9 K. H. Seng, M.-h. Park, Z. P. Guo, H. K. Liu and J. Cho, *Nano Lett.*, 2013, **13**, 1230–1236.
10 J. Hwang, C. Jo, M. G. Kim, J. Chun, E. Lim, S. Kim, S. Jeong, Y. Kim and J. Lee, *ACS Nano*, 2015, **9**, 5299–5309.
11 M. A. Franzman, C. W. Schlenker, M. E. Thompson and R. L. Brutchey, *J. Am. Chem. Soc.*, 2010, **132**, 4060–4061.
12 L. Li, Z. Chen, Y. Hu, X. Wang, T. Zhang, W. Chen and Q. Wang, *J. Am. Chem. Soc.*, 2013, **135**, 1213–1216.
13 F. Q. Wang, S. Zhang, J. Yu and Q. Wang, *Nanoscale*, 2015, **7**, 15962–15970.
14 W. J. Baumgardner, J. J. Choi, Y.-F. Lim and T. Hanrath, *J. Am. Chem. Soc.*, 2010, **132**, 9519–9521.
15 D. D. Vaughn, S.-I. In and R. E. Schaak, *ACS Nano*, 2011, **5**, 8852–8860.
16 J.-J. Wang, A.-F. Lv, Y.-Q. Wang, B. Cui, H.-J. Yan, J.-S. Hu, W.-P. Hu, Y.-G. Guo and L.-J. Wan, *Sci. Rep.*, 2013, **3**, 2613.
17 H. Ju and J. Kim, *ACS Nano*, 2016, **10**, 5730–5739.
18 S. Zhao, H. Wang, Y. Zhou, L. Liao, Y. Jiang, X. Yang, G. Chen, M. Lin, Y. Wang, H. Peng and Z. Liu, *Nano Res.*, 2015, **8**, 288–295.
19 Y. Huang, L. Li, Y.-H. Lin and C.-W. Nan, *J. Phys. Chem. C*, 2017, **121**, 17530–17537.
20 A. Ambrosi and M. Pumera, *Chem. Soc. Rev.*, 2018, **47**, 7213–7224.
21 A. G. Kelly, T. Hallam, C. Backes, A. Harvey, A. S. Esmaeily, I. Godwin, J. Coelho, V. Nicolosi, J. Lauth, A. Kulkarni, S. Kinge, L. D. A. Siebbeles, G. S. Duesberg and J. N. Coleman, *Science*, 2017, **356**, 69–73.
22 Z. Lin, Y. Liu, U. Halim, M. Ding, Y. Liu, Y. Wang, C. Jia, P. Chen, X. Duan, C. Wang, F. Song, M. Li, C. Wan, Y. Huang and X. Duan, *Nature*, 2018, **562**, 254–258.
23 J. Li, C. Chen, S. Liu, J. Lu, W. P. Goh, H. Fang, Z. Qiu, B. Tian, Z. Chen, C. Yao, W. Liu, H. Yan, Y. Yu, D. Wang, Y. Wang, M. Lin, C. Su and J. Lu, *Chem. Mater.*, 2018, **30**, 2742–2749.
24 G. Han, S. R. Popuri, H. F. Greer, J.-W. G. Bos, W. Zhou, A. R. Knox, A. Montecucco, J. Siviter, E. A. Man, M. Macauley, D. J. Paul, W.-g. Li, M. C. Paul, M. Gao, T. Sweet, R. Freer, F. Azough, H. Baig, N. Sellami, T. K. Mallick and D. H. Gregory, *Angew. Chem., Int. Ed.*, 2016, **55**, 6433–6437.
25 J. Jiang, C. P. Y. Wong, J. Zou, S. Li, Q. Wang, J. Chen, D. Qi, H. Wang, G. Eda and D. H. Chua, *2D Mater.*, 2017, **4**, 021026.
26 Z. Qiu, H. Fang, A. Carvalho, A. S. Rodin, Y. Liu, S. J. R. Tan, M. Telychko, P. Lv, J. Su, Y. Wang, A. H. Castro Neto and J. Lu, *Nano Lett.*, 2017, **17**, 6935–6940.
27 S.-u. Kim, A.-T. Duong, S. Cho, S. H. Rhim and J. Kim, *Surf. Sci.*, 2016, **651**, 5–9.
28 H.-Y. Song and J.-T. Lü, *Chem. Phys. Lett.*, 2018, **695**, 200–204.
29 C. W. Li, J. Hong, A. F. May, D. Bansal, S. Chi, T. Hong, G. Ehlers and O. Delaire, *Nat. Phys.*, 2015, **11**, 1063.
30 G. D. Park, J. S. Cho, J.-K. Lee and Y. C. Kang, *Sci. Rep.*, 2016, **6**, 22432.
31 S. Yang, Y. Liu, M. Wu, L.-D. Zhao, Z. Lin, H.-c. Cheng, Y. Wang, C. Jiang, S.-H. Wei, L. Huang, Y. Huang and X. Duan, *Nano Res.*, 2018, **11**, 554–564.
32 H. R. Chandrasekhar, R. G. Humphreys, U. Zwick and M. Cardona, *Phys. Rev. B: Solid State*, 1977, **15**, 2177–2183.
33 Z. Xiao, X. Haiming, L. Zhengdong, T. Chaoliang, L. Zhimin, L. Hai, L. Jiadan, S. Liqun, C. Wei, X. Zhichuan, X. Linghai, H. Wei and Z. Hua, *Angew. Chem., Int. Ed.*, 2015, **54**, 3653–3657.
34 X. Shengjie, L. Dian and W. Peiyi, *Adv. Funct. Mater.*, 2015, **25**, 1127–1136.
35 Z. Xiang Huang, B. Liu, D. Kong, Y. Wang and H. Ying Yang, *Energy Storage Materials*, 2018, **10**, 92–101.
36 Y. Shuang, Z. Yun-Hai, L. Wang, W. Sai, X. Dan, L. Lin, Z. Yu and Z. Xin-Bo, *Adv. Mater.*, 2017, **29**, 1602469.
37 Y. Zhou, *J. Mater. Chem. A*, 2016, **4**, 10906–10913.
38 D.-H. Lee and C.-M. Park, *ACS Appl. Mater. Interfaces*, 2017, **9**, 15439–15448.
39 S. Yuan, Y.-H. Zhu, W. Li, S. Wang, D. Xu, L. Li, Y. Zhang and X.-B. Zhang, *Adv. Mater.*, 2017, **29**, 1602469.
40 K. Tang, L. Fu, R. J. White, L. Yu, M.-M. Titirici, M. Antonietti and J. Maier, *Adv. Energy Mater.*, 2012, **2**, 873–877.
41 S.-Y. Lang, Y. Shi, Y.-G. Guo, D. Wang, R. Wen and L.-J. Wan, *Angew. Chem., Int. Ed.*, 2016, **55**, 15835–15839.
42 W. G. Wang, X. Wang, L. Y. Tian, Y. L. Wang and S. H. Ye, *J. Mater. Chem. A*, 2014, **2**, 4316–4323.

